C.P. No. 446
(20,189)
A.R.C. Technical Report

C.P. No. 446
(20,189)
A.R.C. Technical Report

MINISTRY OF SUPPLY

AERONAUTICAL RESEARCH COUNCIL

CURRENT PAPERS

A One-Dimensional Theory of Liquid-Fuel Rocket Combustion.

Part II. The Influence of Chemical Reaction

by

J. Adler,
Imperial College, London

LONDON: HER MAJESTY'S STATIONERY OFFICE

1959

Price 2s. 6d. net

C.P. No.446

A One-Dimensional Theory of Liquid-Fuel Rocket Combustion II: The Influence of Chemical Reaction

- By -
J. Adler,
Mechanical Engineering Department,
Imperial College, London

28th May, 1958

SUMMARY

The differential equations, resulting from the one-dimensional liquid-fuel rocket combustion Model II of Spalding, have been integrated, and temperature and velocity profiles for the fuel droplets derived. A simple approximate procedure for solving the equations is also given which gives good results when compared with exact integration.

1. Introduction

In a previous paper, Spalding[1], has considered a one-dimensional model for liquid-fuel rocket combustion. By use of laws for droplet vaporisation and drag and the conservation of energy it has been possible to set up first order total differential equations for the temperature, droplet radius and velocity. In these equations the independent variable is the distance of the droplets from the point of injection. To facilitate the derivation of solutions certain simplifying assumptions were made. If the chemical loading parameter, L, is taken as zero, Model I of Spalding's paper, the temperature along the length of the combustion chamber is uniform and equal to the equilibrium gas temperature. An additional simplification is obtained by assuming that Stokes' Law is applicable for the droplet drag, Model I(a), in which case the equations may easily be integrated to give analytical solutions. It has been shown that the qualitative behaviour of these solutions is what one would expect from physical considerations. If L is not zero, chemical reaction is of importance in determining the behaviour of the droplets. Since under practical liquid-fuel rocket operating conditions chemical reaction is likely to be of importance it is necessary to determine what its effect is on the overall performance and in particular whether the solutions of Model I are of sufficient accuracy as L approaches its critical value L_c. The nature of the initial differential equations is such as to make desk computation impracticable and it has therefore been found necessary to programme a high-speed electronic digital computer for their solution.

2./

2. Differential Equations

2.1 Dimensionless form of equations

The differential equations for the droplet radius, velocity, and temperature and the equation for the gas velocity may be put in the following convenient dimensionless form, c.f. Ref. 1.

$$\chi \frac{d\zeta}{d\xi} = -\sigma \beta f_1 \qquad \ldots(1)$$

$$\chi \frac{d\chi}{d\xi} = m \frac{S}{\zeta^2} f_2 \left[\frac{1-\zeta^3}{\delta} - \chi \right] \qquad \ldots(2)$$

$$\frac{d\tau}{d\xi} = \frac{1}{L} \frac{\psi}{1-\zeta^3} - 3\tau\sigma \frac{\zeta^2}{1-\zeta^3} \frac{\beta f_1}{\chi} \qquad \ldots(3)$$

$$\omega = \frac{1-\zeta^3}{\delta} \qquad \ldots(4)$$

in which the symbols have the following meanings:

ζ	dimensionless droplet radius
χ	dimensionless droplet velocity
ξ	dimensionless distance variable
$\beta(\zeta,\chi-\omega)$	dimensionless vaporisation rate
S	dimensionless droplet drag (constant)
ω	dimensionless gas velocity
L	dimensionless chemical loading parameter (constant)
τ	dimensionless temperature or reactedness
$\sigma(\tau)$	functional dependence of vaporisation on reactedness
$m(\tau)$	functional dependence of drag on reactedness
$\delta(\tau)$	functional dependence of gas density on reactedness
$\psi(\tau)$	dimensionless reaction rate function
$f_1[\delta\zeta \lvert\chi-\omega\rvert Re_o/m]$	function of droplet Reynolds number Re
$f_2[\delta\zeta \lvert\chi-\omega\rvert Re_o/m]$	function of droplet Reynolds number Re

Since the dimensionless distance variable does not occur explicitly in the equations it may be eliminated by combining (1) with (2) and (3). One obtains

$$\left| \frac{d\chi}{d\zeta} \right|$$

$$\frac{d\chi}{d\zeta} = -S\,\frac{m}{\sigma}\,\frac{1}{\beta\zeta^2}\left(\frac{f_2}{f_1}\right)\left[\frac{1-\zeta^3}{\delta} - \chi\right] \qquad \ldots(5)$$

$$\frac{d\tau}{d\zeta} = -\frac{1}{(1-\zeta^3)}\left[\frac{1}{L}\,\frac{\psi}{\sigma}\,\frac{\cdot\,\chi}{\beta f_1} - 3\zeta^2\,\tau\right]. \qquad \ldots(6)$$

2.2 Combustion Model II(a)

Spalding has shown that if $Re < 30$ the ratio f_2/f_1 does not differ by more than about 6% from unity. We therefore take this ratio to be unity. If in addition it is assumed that for the particle drag Stokes' Law is operative one will have $f_2 = 1$. We make the further assumptions, that

$$\sigma(\tau) = \tau \qquad \ldots(7)$$

$$m(\tau) = 1 \qquad \ldots(8)$$

$$\delta(\tau) = 1 \qquad \ldots(9)$$

$$\beta = \frac{1}{\zeta}. \qquad \ldots(10)$$

Equations (8) and (9) imply that the gas viscosity and density do not depend explicitly on temperature. Equation (10) arises under pure vaporisation conditions, cf., Ref. 2.

To conform with the definition of the reaction rate function we shall take

$$\psi(\tau) = (n+1)\left(1 + \frac{1}{n}\right)^n (1-\tau)\tau^n \qquad \ldots(11)$$

with n integer. This function has a single maximum and rises from zero to unity and returns to zero as τ goes from zero to unity. It has the form of a typical reaction rate function, cf., Ref. 3.

With conditions (7) - (10) the differential equations become

$$\frac{d\chi}{d\zeta} = -\frac{S}{\tau\zeta}(1 - \zeta^3 - \chi) \qquad \ldots(12)$$

$$\frac{d\tau}{d\zeta} = -\frac{\zeta}{(1-\zeta^3)}\left(\frac{1}{L}\,\frac{\psi}{\tau}\,\chi - 3\zeta\tau\right). \qquad \ldots(13)$$

2.3 Boundary conditions

At the point of droplet injection the following conditions apply:

$$\zeta = 1 : \chi = \chi_0; \quad \tau = \tau_0 \qquad \ldots(14)$$

where τ_0 is determined by the requirement

$$\zeta = 1/$$

$$\zeta = 1 : \frac{d\tau}{d\zeta} = \left(\frac{d\tau}{d\zeta}\right)_1 \equiv \text{finite.} \qquad \ldots(15)$$

Examination of (13) shows that for this to be satisfied one must have

$$\frac{1}{L}\frac{\psi(\tau_0)}{\tau_0}\chi_0 - 3\tau_0 = 0. \qquad \ldots(16)$$

Equation (16) determines real values of τ_0 only if the loading parameter L lies between zero and a critical value L_c. For the reaction rate function (11)

$$L_c = \tfrac{1}{3}\left(\frac{n+1}{n-1}\right)\left(1+\frac{1}{n}\right)^n\left(1-\frac{1}{n-1}\right)^{n-2}\chi_0. \qquad \ldots(17)$$

The functional relationship between L_c/χ_0 and n is shown in Fig. 1.

By application of L'Hospital's theorem to equation (13) at $\zeta = 1$ one can determine (15). With (11) one obtains

$$\left(\frac{d\tau}{d\zeta}\right)_1 = \frac{(S-\tau_0)(1-\tau_0)}{1-(n-2)(1-\tau_0)}. \qquad \ldots(18)$$

At the point of disappearance of the droplet,

$$\zeta = 0 : \chi = 1, \quad \tau = \tau_1 \leqslant 1. \qquad \ldots(19)$$

By integration of (1) with appropriate substitution, it is seen that this occurs at a distance

$$\xi^* = \int_0^{\prime} \frac{\chi}{\tau}\zeta\, d\zeta \qquad \ldots(20)$$

from the point of injection.

2.4 Numerical procedure

To facilitate the forward step-by-step integration of equations (12) and (13) it is convenient to replace ζ by an auxiliary variable. We therefore make the substitution

$$\zeta = 1 - \eta \qquad \ldots(21)$$

so that (12) and (13) become

$$\frac{d\chi}{d\eta} = \frac{S}{(1-\eta)\tau}\left[\eta(\eta^2 - 3\eta + 3) - \chi\right] \qquad \ldots(22)$$

$$\frac{d\tau}{d\eta} = \frac{(1-\eta)}{\eta(\eta^2-3\eta+3)}\left[\frac{1}{L}\frac{\psi}{\tau}\chi - 3(1-\eta)\tau\right]. \qquad \ldots(23)$$

With/

With new boundary conditions:

$$\left.\begin{aligned} \eta = 0 : \chi = \chi_0, \quad \tau = \tau_0 \\ \frac{d\tau}{d\eta} = \left(\frac{d\tau}{d\eta}\right)_0 = \frac{(S - \tau_0)(1 - \tau_0)}{(n - 2)(1 - \tau_0) - 1} \end{aligned}\right\} . \qquad \ldots(24)$$

A Ferranti Mark I* high-speed computer was programmed to deal with the step-by-step integration of equations (22) and (23). The programme employs Gill's form of the Runge-Kutta process[4] which is of fourth order. Unfortunately the method is not applicable to (23) at $\eta = 0$ so that it was necessary to start the integration procedure away from the boundary. The values of the functions at the first step were taken as

$$\chi_1 = \chi_0 + \left(\frac{d\chi}{d\eta}\right)_0 h \qquad \ldots(25)$$

$$\tau_1 = \tau_0 + \left(\frac{d\tau}{d\eta}\right)_0 h \qquad \ldots(26)$$

in which h is the step size for the integration. Since the right-hand side of (22) becomes indeterminate at $\eta = 1$ the integration process was terminated at $\eta = 1 - h$.

3. An Approximate Solution

Equation (16) shows that as $L \to 0$, $\tau_0 \to 1$ and hence that $\left(\frac{d\tau}{d\zeta}\right)_1 \to 0$. Since τ is a monotonic function of ζ for most of $0 \leqslant \zeta \leqslant 1$, a reasonable approximation to make, when $L \ll 1$ is

$$-p = \frac{d\tau}{d\zeta} = 0 \quad \text{in} \quad 0 \leqslant \zeta \leqslant 1. \qquad \ldots(27)$$

Equation (13) now becomes

$$\frac{\psi(\tau)}{\tau^2} - 3\frac{L\zeta}{\chi} = 0. \qquad \ldots(28)$$

For a given ζ and $\chi(\zeta)$, $\tau(\zeta)$ is determined from (28). This value of τ may then be used for a new step in the integration of (12), giving a next value $\chi(\zeta)$. Continuation of the process eventually results in $\chi(\zeta)$ and $\tau(\zeta)$ profiles.

Examination of (28) shows that all $\tau(\zeta)$ profiles pass through $\tau = 1$ when $\zeta = 0$, so that for L not very small, the approximation will overestimate τ for most of its range. On rearrangement of (13)

$$\frac{L}{\chi}\left[3\zeta\tau + p\frac{(1 - \zeta^3)}{\zeta}\right] = \frac{\psi(\tau)}{\tau}. \qquad \ldots(29)$$

In/

In the region where $p < 0$, $p = 0$ underestimates τ and where $p > 0$, $p = 0$ gives an overestimate it being assumed that the change in χ can be neglected. The total effect, as shown by Figs. 2(a) and 2(b), is to displace the profile towards the injection end.

Equation (22) has been integrated in combination with (28) to determine the accuracy of the approximation. Since (22) is a linear differential equation this could easily have been done by use of a desk machine, but since only few modifications to the Mark I* programme were necessary, the calculation was completed using the high-speed computer.

4. Results

Equations (12) and (13) have been integrated for the following parameters:

$$\chi_o = 0.5 \qquad n = 4, 8$$

$$\chi_o = 1 \qquad n = 4, 8.$$

The values of L have been chosen so that in all cases $L < L_c$. As shown by Fig. 1, L_c is a function of χ_o and n. In every case the choice $S = 1$ has been made. Figs. 3(a) and (b) show the results for $\chi_o = 0.5$ and Figs. 4(a) and (b) those for $\chi_o = 1$.

Equation (22) has been integrated in combination with (28) for the particular case:

$$S = 1 \qquad \chi_o = 0.5 \qquad n = 4 \qquad L = 0.25.$$

The resulting curves are shown in Fig. 5. The corresponding exact integration is also again displayed for comparison.

All curves have been plotted against $\eta = 1 - \zeta$. If Γ_o is the droplet radius at injection and Γ the radius at any subsequent position, then

$$\eta = \frac{\Gamma_o - \Gamma}{\Gamma_o} \qquad \ldots(30)$$

so that η is the fractional decrease in the droplet radius.

Values of ζ^* have been evaluated using equation (20) and are shown on Figs. 3 - 5.

5. Discussion

Examination of the temperature profiles of Figs. 3 - 4 shows that τ is nearly in all cases a monotonic function of η. When the loading parameter is close to its critical value there is an initial drop in temperature which then rises to its maximum value τ_1. As τ_1 is less than unity, chemical reaction is incomplete at the point of disappearance of the droplets and an additional distance is required for the process to go to completion. This distance, which has not been evaluated, should be added to ζ^* to give the minimum rocket length for efficient combustion.

The droplet velocity profiles show that for given initial conditions they are nearly independent of variations in the loading parameter. This indicates that Model I(a) of Spalding will give good results even when L is not zero. All velocities initially fall below

those/

those at the point of injection, and as previously, reach the gas velocity at the disappearance of the droplets.

The values of ξ^* are increasing functions of the loading parameter L. This, as may be seen, is due to an overall drop in temperature as L increases.

The maximum chemical loading L_c, is determined by the shape of the reaction rate function, characterized by n, and by χ_o, the injection velocity of the droplets. Equation (17) shows that L_c increases linearly with χ_o and decreases with increasing activation energy.

Examination of the approximate solutions, plotted in Fig. 5, shows that the velocity profile is practically coincident with that given by exact integration. The temperature profile, as predicted, lies slightly above the exact solution, but this discrepancy will disappear with decreasing L and increasing n.

Acknowledgements

The author wishes to thank Dr. D. B. Spalding for suggesting the problem and for helpful discussions. Thanks are also due to A.R.D.E., Fort Halstead for use of the electronic digital computer AMOS.

References

No.	Author(s)	Title, etc.
1	D. B. Spalding	A one-dimensional theory of liquid-fuel rocket combustion. C.P.445. May, 1958.
2	D. B. Spalding and V. K. Jain	Theory of the burning of mono-propellant droplets. C.P.447. May, 1958.
3	D. B. Spalding	Combustion and flame 1 (1957) 287, 296.
4	S. Gill	Proc. Camb. Phil. Soc. 47 (1950) 96.

FIG. 1.

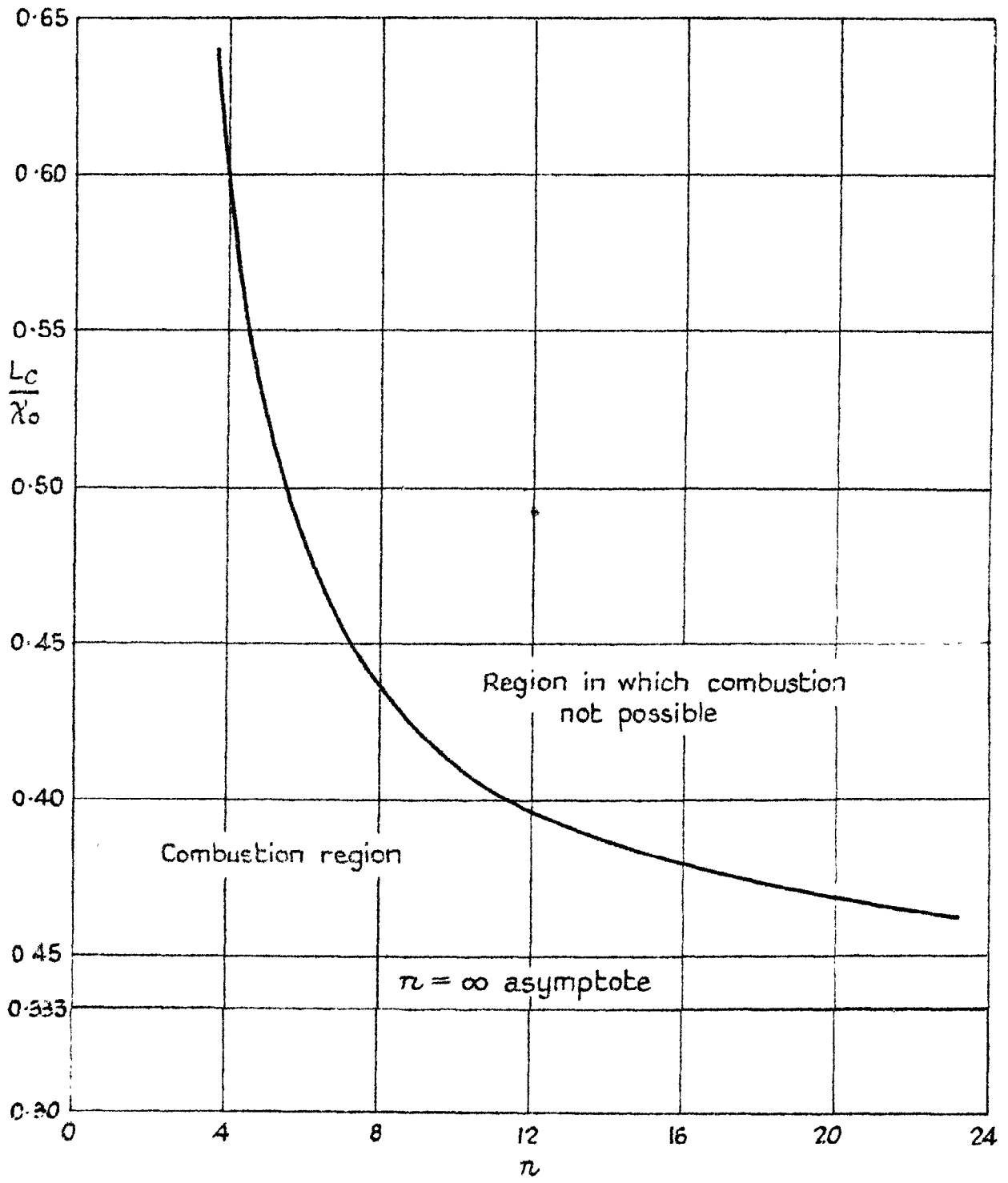

$\frac{L_c}{\chi_0}$ versus reaction rate function paramenter n of the system

$$\psi(\tau) = (n+1)\left(1+\tfrac{1}{n}\right)^n (1-\tau)\,\tau^n$$

FIG. 2 (a & b)

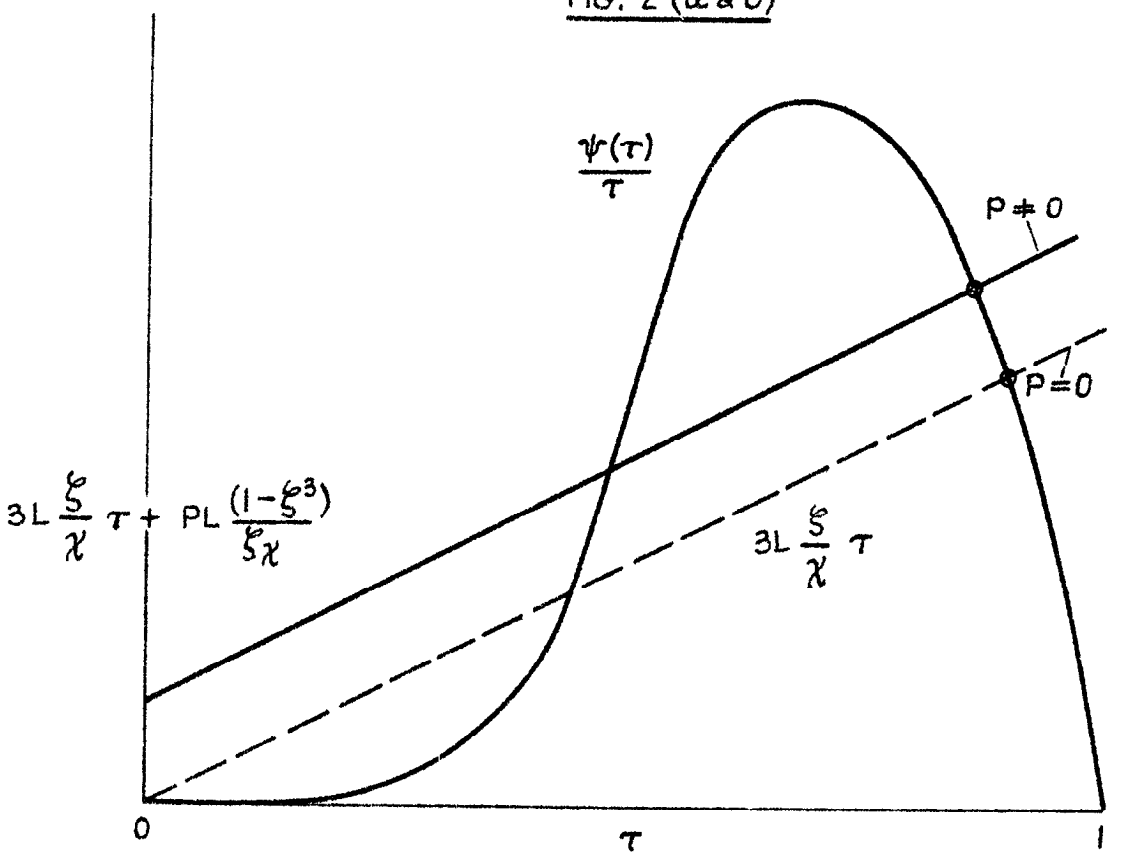

(a)

Graphical construction for determining τ from typical reaction rate function $\psi(\tau)$

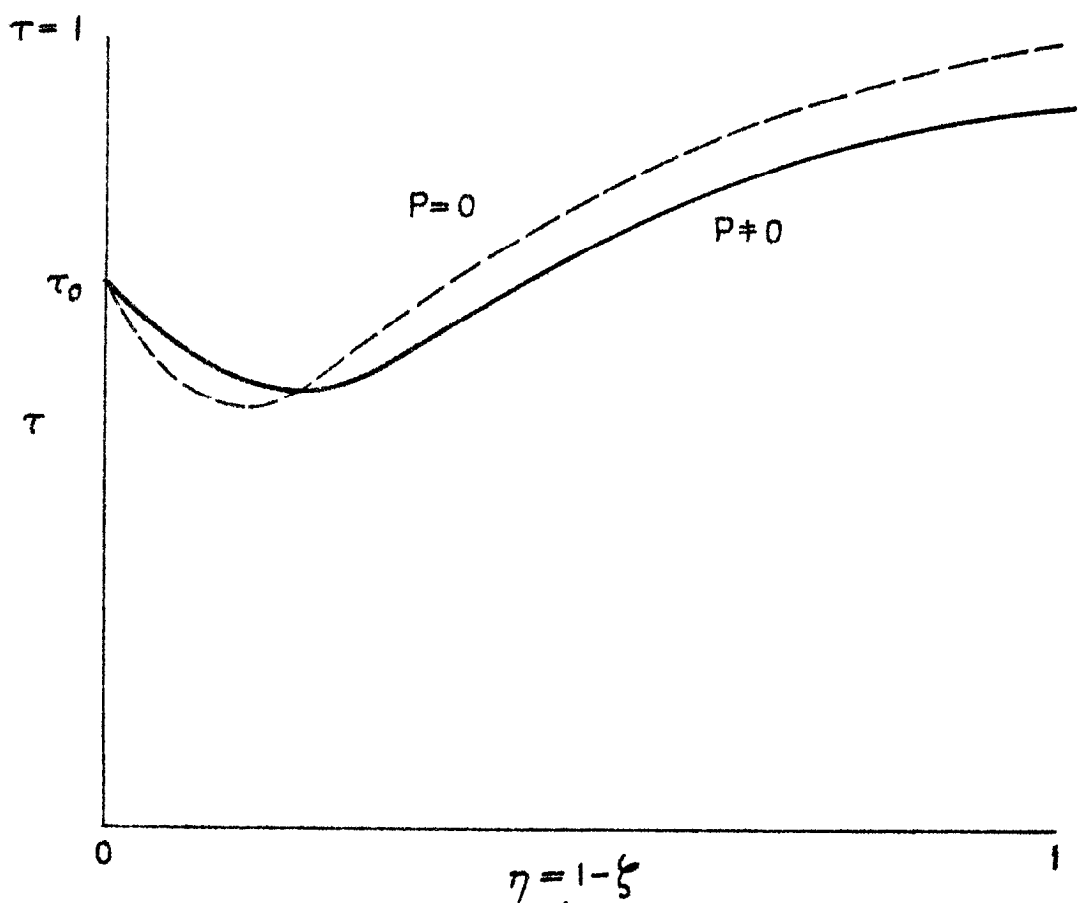

(b)

Typical τ versus ξ curve showing effect of neglecting temperature gradient P.

FIG. 3 (a)

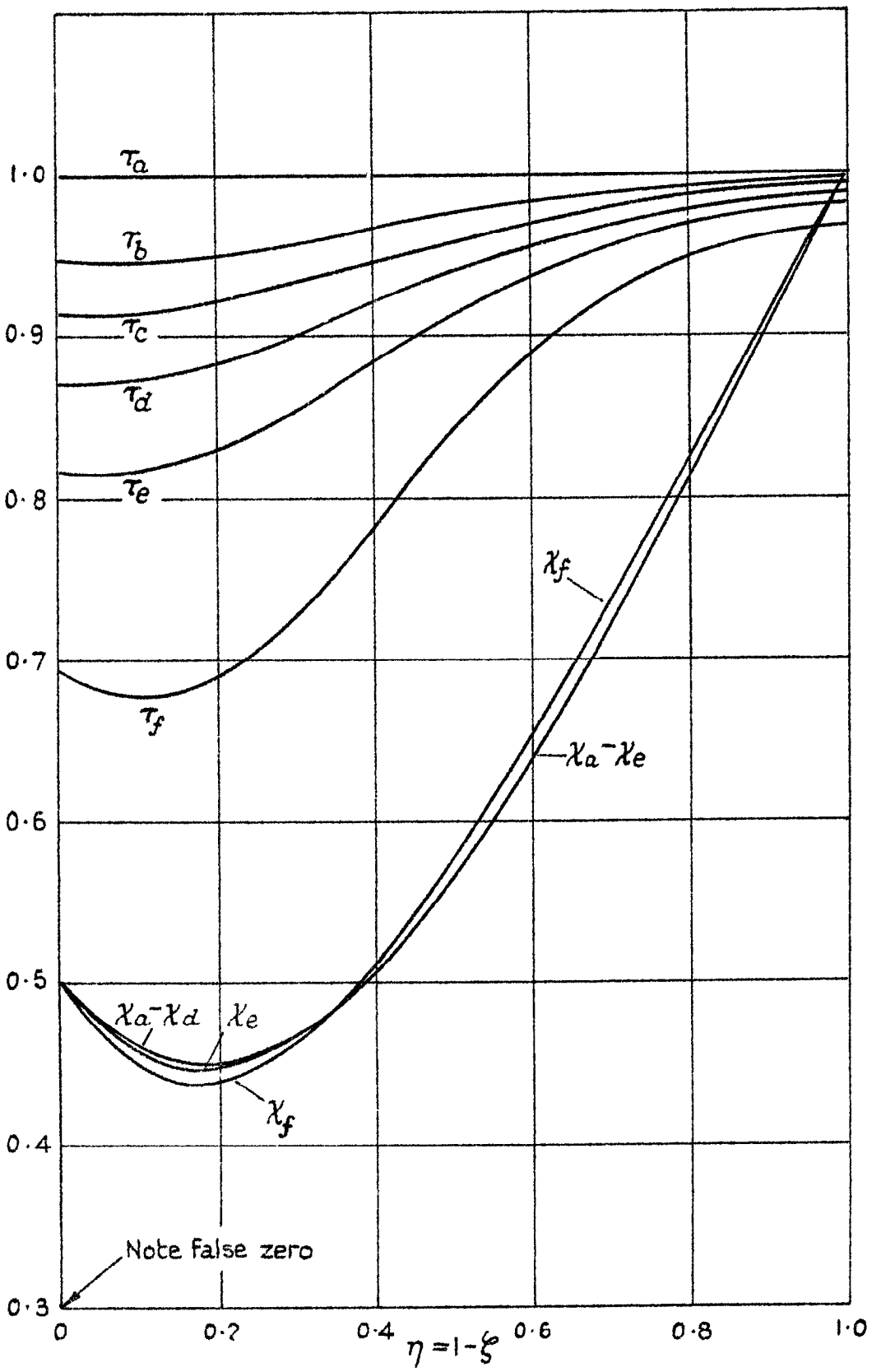

τ and χ versus η curves for $\chi_0 = 0{\cdot}5$ $n = 4$.

τ_a	χ_a :	L = 0 ,	$\xi^* = 0{\cdot}267$
τ_b	χ_b :	L = 0·10 ,	$\xi^* = 0{\cdot}276$
τ_c	χ_c :	L = 0·15 ,	$\xi^* = 0{\cdot}282$
τ_d	χ_d :	L = 0·20 ,	$\xi^* = 0{\cdot}291$
τ_e	χ_e :	L = 0·25 ,	$\xi^* = 0{\cdot}304$
τ_f	χ_f :	L = 0·30 ,	$\xi^* = 0{\cdot}344$

FIG. 3(b)

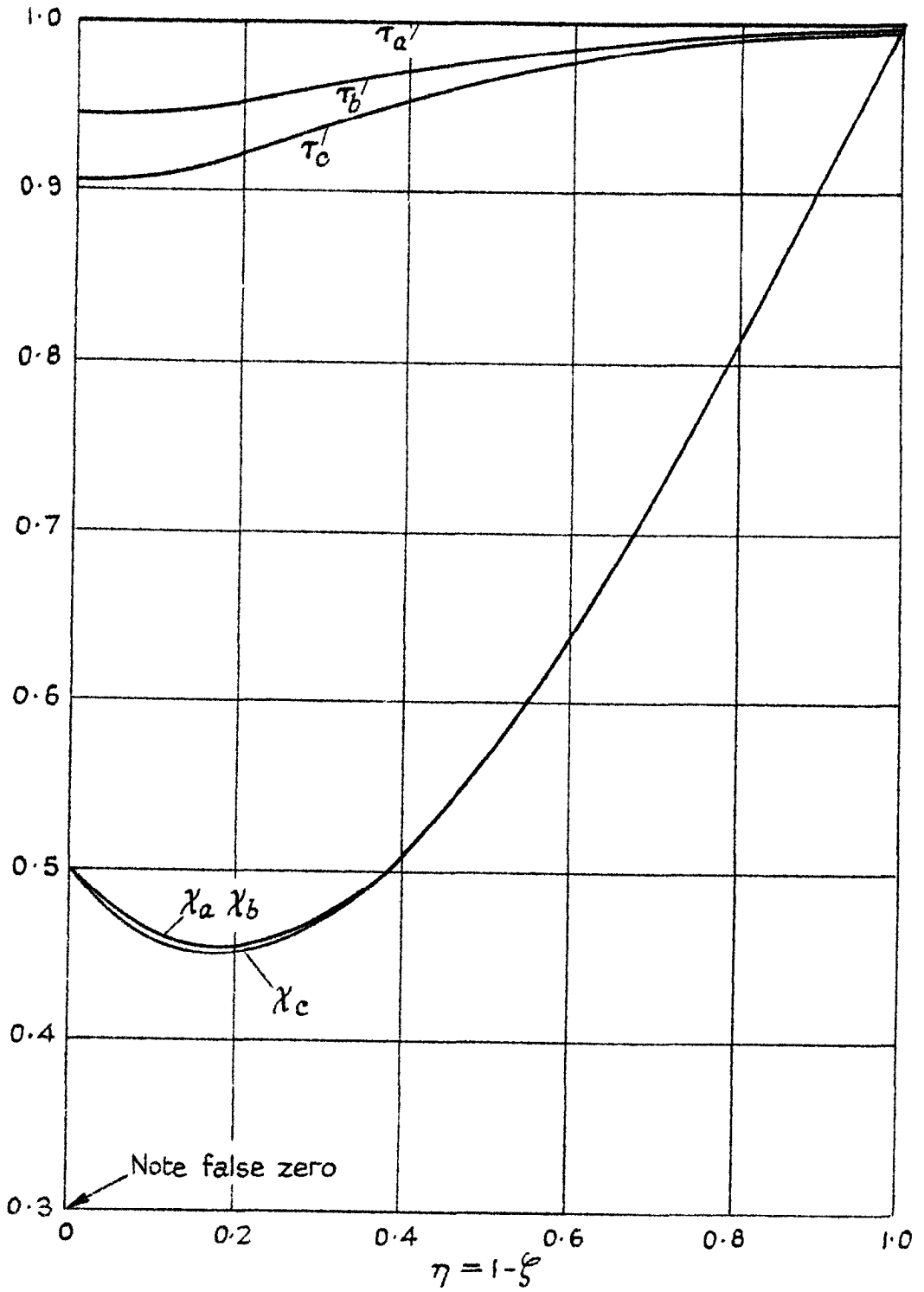

τ and χ versus η curves for $\chi_0 = 0{\cdot}5$ $n = 8$.

τ_a χ_a : L = 0 $\xi^* = 0{\cdot}267$
τ_b χ_b : L = 0·15, $\xi^* = 0{\cdot}275$
τ_c χ_c : L = 0·20, $\xi^* = 0{\cdot}281$

FIG. 4 (a)

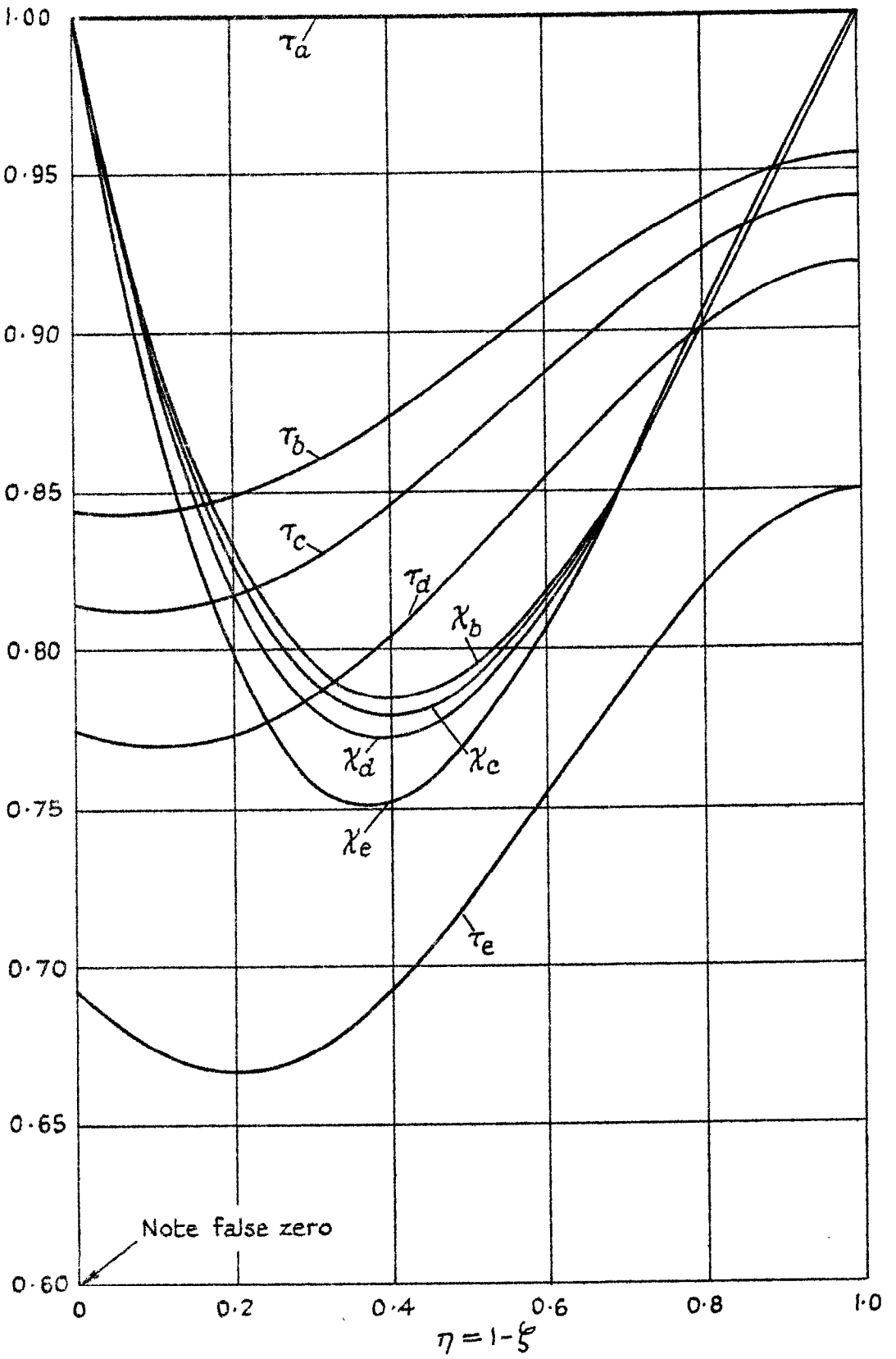

τ and χ versus η curves for $\chi_0 = 1 \quad n = 4$

τ_a	:	L = 0 ,	$\xi^* = 0.433$
τ_b , χ_b	:	L = 0·45,	$\xi^* = 0.502$
τ_c , χ_c	:	L = 0·50,	$\xi^* = 0.517$
τ_d , χ_d	:	L = 0·55,	$\xi^* = 0.539$
τ_e , χ_e	:	L = 0·60,	$\xi^* = 0.606$

FIG. 4 (b)

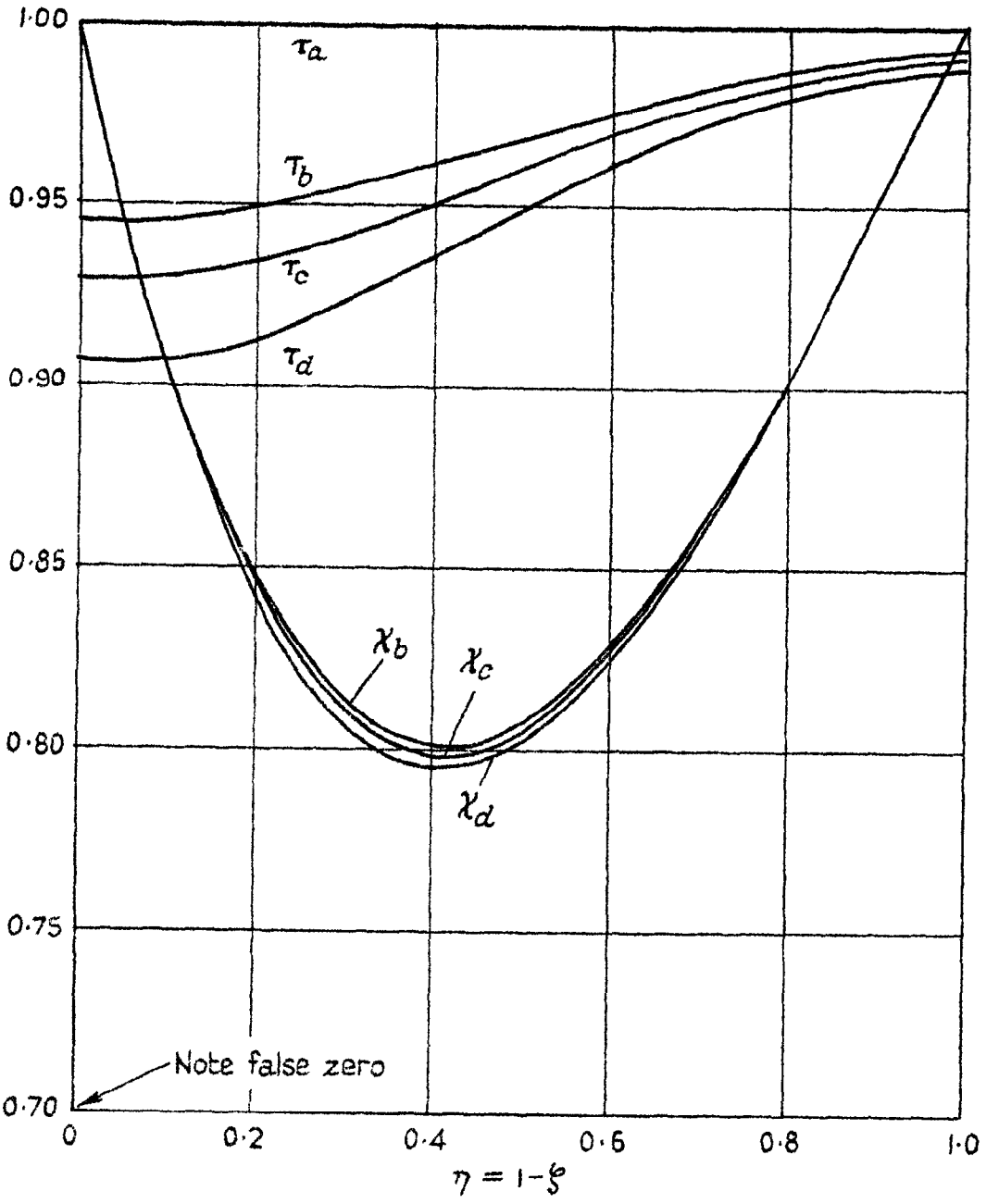

τ and χ versus η curves for $\chi_0 = 1$ $n = 8$

τ_a	:	L = 0	$\xi^* = 0{\cdot}433$
τ_b χ_b	:	L = 0·30,	$\xi^* = 0{\cdot}463$
τ_c χ_c	:	L = 0·35,	$\xi^* = 0{\cdot}468$
τ_d χ_d	:	L = 0·40,	$\xi^* = 0{\cdot}475$

FIG. 5.

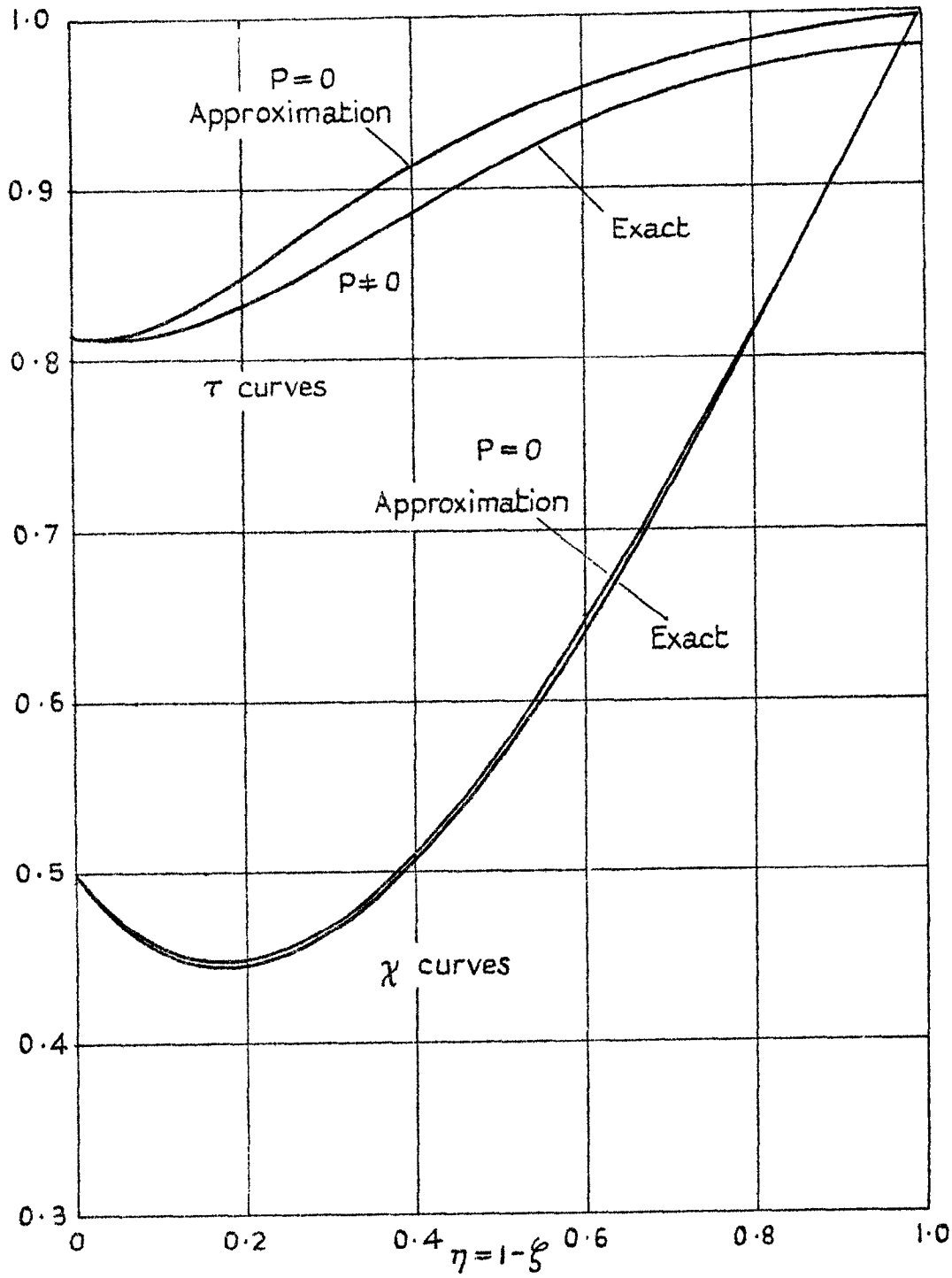

τ and χ versus η curves for $\chi_0 = 0{\cdot}5$ $n = 4$ $L = 0{\cdot}25$ showing effect of neglecting temperature gradient P.

Exact integration $\xi^* = 0{\cdot}304$
P = 0 approximation $\xi^* = 0{\cdot}298$

C.P. No. 446
(20,189)
A.R.C. Technical Report

Printed and published by
HER MAJESTY'S STATIONERY OFFICE

To be purchased from
York House, Kingsway, London W.C.2
423 Oxford Street, London W.1
13A Castle Street, Edinburgh 2
109 St Mary Street, Cardiff
39 King Street, Manchester 2
Tower Lane, Bristol 1
2 Edmund Street, Birmingham 3
80 Chichester Street, Belfast
or through any bookseller

Printed in Great Britain

S.O. Code No. 23-9011-46

C.P. No. 446